INVITED PAPER

PACS numbers: 32.10.Fn; 12.20.Fv; 42.50.Xa
DOI: 10.1070/QE2005v035n03ABEH002871

Hyperfine structure of the metastable level in hydrogen-like atoms

N.N. Kolachevsky

***Abstract*. Precision methods for measuring the hyperfine splitting $E_{\rm HFS}(2S)$ of the metastable level in light hydrogen-like systems such as hydrogen, deuterium, and the $^3He^+$ ion are considered. These measurements open up a new possibility for precise testing of quantum electrodynamics (QED) of bound states in hadronic systems. While the direct calculation of the energy levels in such systems runs into the problem of the uncertainty of the nuclear charge radius, the contribution of energy corrections appearing in the calculation of the parameter $D_{21} = 8E_{\rm HFS}(2S) - E_{\rm HFS}(1S)$ taking the finite size of the nucleus into account becomes smaller. The results of calculations of D_{21} are presented and compared with experimental values. The approach considered in the paper allows the testing of some bound-state QED corrections to the hyperfine splitting energy at a level of 10^{-7}, which is comparable with the results of precision QED tests based on the study of the hyperfine splitting in leptonic systems.**

Keywords: *quantum electrodynamics, hydrogen-like system, hyperfine structure, metastable level, precision spectroscopy.*

1. Introduction

The appearance and development of quantum electrodynamics (QED) is closely associated with precision spectroscopic experiments performed with a hydrogen atom and a number of hydrogen-like atoms. One of the most sensitive and illustrative QED tests of bound states is the study of the Lamb shift in light hydrogen-like systems [1]. At present the QED calculations of bound states are used for determining a number of fundamental quantities such as the Rydberg constant $R_\infty = m_e e^4/2\hbar^2$ (m_e is the electron mass) [2], the fine structure constant $\alpha = e^2/\hbar c$ [3, 4], and many others [5]. A significant progress achieved during the last decade in the calculations of multiloop QED corrections and in the improvement of the experimental accuracy of measurements of the anomalous magnetic moment of a bound electron makes it possible to consider the possibility of using this new method for determining the fundamental m_e/m_p ratio [6] (m_p is the proton mass), which is more accurate than the classical measuring method [7].

Despite the success achieved in the calculations of multiloop corrections, the accuracy of energy-level calculations in light hadronic systems (whose nuclei contain quarks) is limited because the nuclear charge radius is known with a limited accuracy. The energy correction for the nS levels of a hydrogen-like system due to a finite size of a nucleus has the form

$$\delta E_{\rm N}(n{\rm S}) = A_{\rm N}\langle r_{\rm N}^2\rangle |\psi_{n{\rm S}}(r=0)|^2, \tag{1}$$

where $\langle r_{\rm N}^2\rangle^{1/2}$ is the root-mean-square nuclear charge radius; $A_{\rm N}$ is a coefficient independent of the principal quantum number n. Because the square of the modulus of the wave function of the S electron on the nucleus is

$$|\psi_{n{\rm S}}(r=0)|^2 = \frac{1}{\pi}\left(\frac{Zm_{\rm r}e^2}{n\hbar^2}\right)^3 \tag{2}$$

(where Z is the nucleus charge; $m_{\rm r} = m_e M/(M+m_e)$ is the reduced electron mass; and M is the nucleus mass), the dependence of the correction $\delta E_{\rm N}(n{\rm S})$ on n will have the same form as the dependences of other corrections to the Lamb shift energy [$\delta E_{\rm N}(n{\rm S}) \propto 1/n^3$], thereby being indistinguishable from QED corrections.

In the case of a hydrogen atom, the accuracy of calculations of the Lamb shift and hyperfine structure is limited by the experimental error of measuring the proton charge radius $\langle r_{\rm p}^2\rangle^{1/2}$. This radius is found from the experiments on electron scattering by protons (see, for example, [8, 9]) and from optical measurements of transition frequencies in a hydrogen atom [10]. Some results of the measurements do not agree with each other within a standard deviation, which requires a conservative increase in the error. In paper [11] devoted to analysis of the data on the proton charge radius, the value $\langle r_{\rm p}^2\rangle^{1/2} = 0.880(15)$ fm is recommended (hereafter, the number in parentheses corresponds to one standard deviation).

The correction $\delta E_{\rm N}(1S)$ to the Lamb shift in hydrogen caused by the proton charge radius is 1167(32) kHz for the ground state. The error of 32 kHz, amounting to 4×10^{-6} of the Lamb shift in the ground state $L_{1S} = 8\,172\,807\times(32+10)$ kHz [2], is determined by the error of measuring the proton charge radius; the error of 10 kHz (the second number in parentheses) corresponds to the contribution of uncalculated QED corrections. One can see that in the study of the Lamb shift, the accuracy of QED tests is manly

N.N. Kolachevsky P.N. Lebedev Physics Institute, Russian Academy of Sciences, Leninskii prosp. 53, 119991 Moscow, Russia;
e-mail: kolach@fromru.com

Received 21 September 2004; revision received 11 November 2004
Kvantovaya Elektronika **35** (3) 207 – 218 (2005)
Translated by M.N. Sapozhnikov

restricted by the error of measuring $\langle r_p^2\rangle^{1/2}$, which makes further calculations of corrections unsuitable. At present, the Lamb shift in the muonic hydrogen atom ($p^+\mu^-$) is being actively studied by the methods of optical spectroscopy, and the appearance of new independent data on the radius $\langle r_p^2\rangle^{1/2}$ is expected [12].

The influence of the nuclear form factor can be reduced by passing to charged one-electron systems with the intermediate charge values $Z \sim 10$. In this case, the relative contribution of some QED corrections increases compared to δE_N (due to the different dependence on Z), which enhances the sensitivity of the QED tests. The g-factor of a bound electron also weakly depends on the nuclear structure. Thus, a great success has been recently achieved in the measurement and calculation of the g-factor of bound electrons in the $^{12}C^{5+}$ [6] and $^{16}O^{7+}$ ions [13] in a Penning trap.

Another possibility is the study of leptonic systems that are free from hadronic effects. The hyperfine splitting in the ground state was precisely measured in muonium Mu (μ^+e^-) [14] and positronium Ps (e^+e^-) [15]. Because these systems are unstable, a special technique is required for their study, which restricts in the general case the measurement accuracy. The QED calculations are in good agreement with the experiment. In particular, for a muonium atom the QED calculations are valid with an accuracy of $\sim 10^{-7}$. However, the sensitivity of QED tests in this case is restricted by the experimental error of measuring the ratio m_μ/m_e of the muon and electron masses [16] entering the expression for the Fermi energy.

The calculation of the hyperfine splitting in hydrogen-like hadronic systems also involves the problem of consideration of the nuclear charge radius. The hyperfine splittings $E_{HFS}(1S)$ in the ground state of stable hydrogen-like systems have been measured very accurately (for the hydrogen atom, the error is 10^{-13} [17]), which can open up wide possibilities for QED tests when the nuclear structure is well known. However, the difference between the values calculated within the framework of a 'pure' QED and the experimental values amounts to 10^{-4}, which do not allow one to judge about the validity of many corrections.

In this paper, the possibility of performing QED tests in hadronic systems is considered which is based on the analysis of the specific energy difference $D_{n'n}$, which is weakly sensitive to the energy contributions caused by a finite size of the nucleus. It was pointed out in a number of papers that if the difference of energies $E(n\mathrm{S})$, corresponding to the different S levels of a hydrogen-like system, is represented in the form

$$D_{n'n} = n'^3 E(n'\,\mathrm{S}) - n^3 E(n\mathrm{S}), \tag{3}$$

the influence of the corresponding corrections $\delta E_N(n\mathrm{S})$ will decrease, as follows from (1) and (2). This conclusion is valid in the relativistic case as well [18]. One of the promising objects for the study is the difference of parameters

$$D_{21} = 8E_{HFS}(2S) - E_{HFS}(1S), \tag{4}$$

because the 2S level of the hydrogen-like system is a long-lived excited level allowing precision hyperfine-splitting measurements.

The accuracy of calculations of corrections to the hyperfine splitting energy and the value of D_{21} has been considerably improved in the last years [19, 20]. The new QED corrections, depending on the principal quantum number n, were calculated up to the terms α^4 and $\alpha^3\times(m_e/m_p)$ inclusive, as well as higher-order small corrections related to the nuclear structure. At present the accuracy of theoretical calculations exceeds the accuracy of measuring D_{21}, which is determined by the experimental error of the splitting energy $E_{HFS}(2S)$ of the not easily accessible excited state, which amounts to tens – hundreds of hertz, and by the error of measuring the ground-state hyperfine splitting in neutral H and D atoms (microhertz). Such a high accuracy of measuring $E_{HFS}(1S)$ allows one to neglect completely the contribution of the error of measuring $E_{HFS}(1S)$ to expression (4).

The hyperfine splitting $E_{HFS}(2S)$ in the hydrogen atom also attracts interest because it is used in the determination of the Rydberg constant R_∞ [2]. One of the experimental parameters required for these measurements is the frequency of the hyperfine centroid of the 1S – 2S transition in the hydrogen atom. However, in spectroscopic experiments (for example, [21]), the optical frequency of the $1S(F=1,\ m_F=\pm1) \rightarrow 2S(F=1,\ m_F=\pm1)$ transition between the magnetic sublevels of hyperfine components is measured. Here, F is the quantum number of the total atomic momentum and m_F is the magnetic quantum number. The centroid frequency is determined by introducing the hyperfine-structure correction $[E_{HFS}(1S) - E_{HFS}(2S)]/4$.

At present the value of D_{21} can be accurately determined for three light hydrogen-like systems: hydrogen, deuterium, and the $^3He^+$ ion.

The ground-state hyperfine splitting $E_{HFS}(1S)$ in hydrogen and deuterium has been determined from the measurements of the maser frequency performed by the Ramsey group [17, 22]. Analysis of these experiments is beyond the scope of this paper. The hyperfine splitting $E_{HFS}(2S)$ has been measured twice by the method of radio-frequency spectroscopy [23, 24] and by the optical method [25]. Radio-frequency [26] and optical measurements [27] have been also performed for deuterium.

The study of the hyperfine splitting of the 1S and 2S levels in the $^3He^+$ ion requires completely new experimental approaches compared to neutral systems. The ground-state hyperfine splitting was measured for ions captured in quadrupole traps and excited by a radio-frequency field; the nuclear spins were oriented in collisions with a beam of polarised cesium atoms [28]. Although the experimental accuracy was quite high (10^{-9}), it is nevertheless significantly inferior to that obtained in experiments with neutral systems. In turn, the relative accuracy of measuring $E_{HFS}(2S)$ in the $^3He^+$ ion is better than in neutral systems. These measurements were performed twice – by a classical method of Ramsey spectroscopy in an ion beam [29] and by the method of microwave excitation in a trap [30]. Note that, from the point of view of QED tests, the $^3He^+$ ion has a natural advantage because its Fermi energy is higher by modulus than that in hydrogen and deuterium by factors of 6 and 25, respectively.

2. Hyperfine structure and the parameter D_{21}

The interaction of the nuclear spin $\boldsymbol{I}$ with the total momentum $\boldsymbol{j}$ of the electron shell results in the level splitting, which

is called the hyperfine splitting. The expression for the energy $E_{\rm HFS}(n,l,j,F)$ derived by Fermi and presented in [31] can be simplified in the case of hydrogen-like atoms. The main nonrelativistic contribution to the hyperfine splitting for a hydrogen-like atom in the nS state is

$$E_{\rm HFS}(n{\rm S}) = \frac{E_F}{n^3}, \tag{5}$$

where the Fermi energy is

$$E_{\rm F} = \frac{8}{3}\, Z^3\alpha^2 hcR_\infty\, \frac{g_{\rm nucl}\mu_{\rm N}}{\mu_{\rm B}}\, \frac{2I+1}{2I} \left(\frac{m_{\rm r}}{m_{\rm e}}\right)^3, \tag{6}$$

where $g_{\rm nucl}$ is the nuclear g-factor; $\mu_{\rm B}$ is the Bohr magneton; and $\mu_{\rm N} = \mu_{\rm B}(m_{\rm e}/m_{\rm p})$ is the nuclear magneton. The nuclear magnetic momentum $g_{\rm nucl}\mu_{\rm N}$ is assumed positive if it is directed along the nuclear spin and negative if it has the opposite direction. Correspondingly, the Fermi energy, which is the difference of energies of the $F = I + 1/2$ and $F = I - 1/2$ states can assume both positive and negative values.

QED opens up the possibilities for systematic calculations of corrections to expression (5). The expansion is performed in small parameters α, $Z\alpha$, and $m_{\rm e}/M$. Similarly to the Lamb shift calculations, the radiative corrections, nonradiative and radiative recoil corrections, etc. are successively calculated. Beginning from a certain accuracy level, the size and structure of the nucleus play an important role for hadronic systems, while for lepton systems the weak interactions become important. The methods of calculation of the main corrections to $E_{\rm F}$ are considered in review [1]. We will consider here only the contributions that depend on the principal quantum number n and for the parameter D_{21}, which can be conveniently represented in the form of an expansion in powers (indices in parentheses) of α and $m_{\rm e}/M$ taking into account a small residual contribution $\delta D_{21}^{\rm nucl}$ of hadronic effects:

$$D_{21} = D_{21}^{(2)} + D_{21}^{(3)} + D_{21}^{(4)} + \delta D_{21}^{\rm nucl}. \tag{7}$$

2.1 Corrections to the hyperfine interaction energy

We assume below that $\hbar = c = 1$. The corrections to the hyperfine splitting energy can have the form

$$E_{\rm HFS}^{\rm QED}(n{\rm S}) = \frac{E_F}{n^3}\, Q_{\rm QED}(n{\rm S}). \tag{8}$$

The quantity $Q_{\rm QED}(n{\rm S}) \approx 1$ takes into account the contribution of the relativistic and radiative corrections, as well as recoil corrections and can be represented in the form

$$Q_{\rm QED}(n{\rm S}) = B_n + a_{\rm e} + \alpha(Z\alpha)C^{(2)} + \frac{\alpha}{\pi}\, D_n^{(2)} + \frac{\alpha^2}{\pi}\,(Z\alpha)C^{(4)} + \left(\frac{\alpha}{\pi}\right)^2 D_n^{(4)} + \ldots \tag{9}$$

The terms B_n are the relativistic Breit corrections which appear upon the expansion of the relativistic root $\sqrt{p^2 + m_{\rm e}^2}$ (p is the electron momentum) in powers of $(Z\alpha)^2$ [32]:

$$\begin{aligned} B_1 &= \frac{1}{\gamma(2\gamma-1)} = 1 + \frac{3}{2}\,(Z\alpha)^2 + \frac{17}{8}\,(Z\alpha)^4 + \ldots, \\ B_2 &= \frac{2\{2(1+\gamma) + [2(1+\gamma)]^{1/2}\}}{\gamma(4\gamma^2-1)(1+\gamma)^2} = 1 + \frac{17}{8}\,(Z\alpha)^2 \\ &\quad + \frac{449}{128}(Z\alpha)^4 + \ldots, \end{aligned} \tag{10}$$

where $\gamma = [1 - (Z\alpha)^2]^{1/2}$; $C^{(2)}$ and $C^{(4)}$ are some coefficients, whose values are determined below. For the ground state of the hydrogen atom, $E_F \simeq 1.42$ GHz, and the relativistic correction is $E_F(B_1 - 1) \simeq 114$ kHz. Naturally, the values of relativistic corrections depend substantially on the principal quantum number and therefore they make the main contribution to the value of D_{21} [see (4) and (7)]:

$$D_{21}^{(2)} = \frac{5}{8}\,(Z\alpha)^2 E_F. \tag{11}$$

The main radiative correction to the hyperfine splitting energy appears due to the anomalous magnetic moment of an electron $a_{\rm e} = (g_{\rm e} - 2)/2$ (in units of the doubled Bohr magneton), where $g_{\rm e}$ is the reduced gyromagnetic ratio for a free electron. The correction coincides with the value of the anomalous magnetic moment of a free electron (see [1, 33]). This results in the appearance of the well-known radiative terms $(\alpha/\pi)E_F$, which are independent of the coupling parameter $Z\alpha$:

$$a_{\rm e} = \frac{1}{2}\left(\frac{\alpha}{\pi}\right) - 0.328478965\ldots\left(\frac{\alpha}{\pi}\right)^2 + 1.181241456\ldots\left(\frac{\alpha}{\pi}\right)^3. \tag{12}$$

Because the corrections $a_{\rm e}$ are independent of n, they disappear in the calculation of the parameter D_{21}.

The next terms of the type $\alpha(Z\alpha)E_F$ appear due to the relation between radiative processes and Coulomb interaction between a nucleus and an electron. The simplest corrections of this type were calculated long ago and are presented in a number of classic papers [34, 35]. These corrections correspond physically to the corrections $\alpha(Z\alpha)^5 m_{\rm e}$ to the Lamb shift because they are related to single-loop processes with two exchange Coulomb photons. The calculations give the coefficient $C^{(2)}$ in (9):

$$C^{(2)} = \left(\ln 2 - \frac{5}{2}\right), \tag{13}$$

which is independent of n and disappears in the calculation of D_{21}.

Corrections of the type $\alpha^2(Z\alpha)$ belong to similar radiative corrections, which are related to two-loop processes. We will not describe them in detail (see [1] and references therein for details) and present here only the numerical value of the coefficient

$$C^{(4)} = 0.7717(4), \tag{14}$$

which determines these corrections for $Q_{\rm QED}(n{\rm S})$ and also is independent of n.

Consider now the next, so-called Zwanziger corrections of the type $\alpha(Z\alpha)^2 E_F$, which already depend on n, thereby making an appreciable contribution to the parameter D_{21} (Fig. 1). The calculations lead to the appearance of logarithmic contributions caused by photons with small momenta of the order of $m_e(Z\alpha)$. The calculations of corrections presented by the left diagram in Fig. 1 are somewhat similar to the calculation of the principal logarithmic term in the Lamb shift of the order $\alpha(Z\alpha)^4 m_e$.

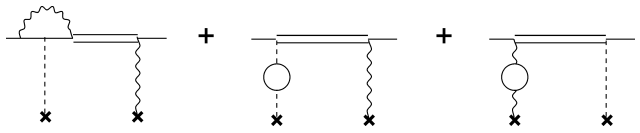

Figure 1. Feynman diagrams describing radiative corrections of the type $\alpha(Z\alpha)^2 E_F$, which make a noticeable contribution to D_{21}. The solid straight lines denote an electron, crosses denote an infinitely heavy nucleus with which the exchange by photons occurs, circles – a virtual electron–positron pair. The dashed straight lines denote Coulomb nonrelativistic photons, the wavy lines denote relativistic photons corresponding to the Breit Hamiltonian. The double solid straight lines correspond to a bound electron and are described by a complete Coulomb Green function. Each of the diagrams should be taken into account twice because of the presence of topological twins.

The 1S and 2S states are characterised by the coefficients

$$D_1^{(2)} = (Z\alpha)^2\left[-\frac{8}{3}\ln^2(Z\alpha) + \left(\frac{16}{3}\ln 2 - \frac{281}{180}\right)\ln(Z\alpha) + G_1^{\mathrm{SE}}(Z\alpha) + G_1^{\mathrm{VP}}(Z\alpha)\right], \tag{15}$$

$$D_2^{(2)} = (Z\alpha)^2\left[-\frac{8}{3}\ln^2(Z\alpha) + \left(\frac{32}{3}\ln 2 - \frac{1541}{180}\right)\ln(Z\alpha) + G_2^{\mathrm{SE}}(Z\alpha) + G_2^{\mathrm{VP}}(Z\alpha)\right]. \tag{16}$$

The value of the function G_1^{SE} (correction to the self-energy) for the hydrogen atom ($Z = 1$) calculated in [36] is 16.079(15), while the function G_1^{VP} (correction for the vacuum polarisation) is known analytically

$$G_1^{\mathrm{VP}} = -\frac{8}{15}\ln 2 + \frac{34}{225} + \pi(Z\alpha)\left[-\frac{13}{24}\ln\frac{Z\alpha}{2} + \frac{539}{288}\right] + \ldots. \tag{17}$$

It is also necessary to present the values of these functions for the 2S level:

$$G_2^{\mathrm{SE}} = G_1^{\mathrm{SE}} - 5.221233(3) + \mathrm{O}(\pi(Z\alpha)),$$
$$G_2^{\mathrm{VP}} = G_1^{\mathrm{VP}} - \frac{7}{10} + \frac{8}{15}\ln 2 + \mathrm{O}(\pi(Z\alpha)). \tag{18}$$

By considering corrections of the type $\alpha^2(Z\alpha)^2 E_F$, it is sufficient to present the result only for the ground state because the contributions to the parameter $D_n^{(4)}$ known at present are independent of n [37, 38]:

$$D_1^{(4)} = -\frac{4}{3}(Z\alpha)^2\ln^2(Z\alpha). \tag{19}$$

The nonradiative recoil corrections to the hyperfine splitting energy of the order of $(Z\alpha)(m_e/M)E_F$ and $(Z\alpha)^2(m_e/M)E_F$, appearing due to a finite mass of the nucleus, are similar to the corrections $(Z\alpha)^5(m_e/M)m_e$ and $(Z\alpha)^6(m_e/M)m_e$ to the Lamb shift and are determined with the help of diagrams presented in Fig. 2.

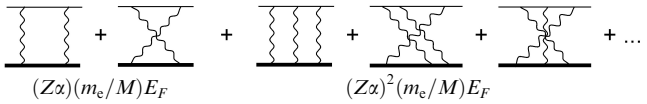

Figure 2. Basic nonradiative recoil corrections to the hyperfine-splitting energy. The thin solid straight lines denote an electron, the thick straight lines denote a nucleus with a finite mass experiencing the recoil, the wavy lines denote relativistic photons corresponding to the Breit Hamiltonian.

Corrections of this type were calculated by different authors in the 1980s (see review [1]), and their differential contribution to D_{21} was determined by Sternheim [39]:

$$\delta D_{21}^{\mathrm{rec}} = (Z\alpha)^2 E_F \frac{m_e}{m_p}\left\{-\frac{9}{8} + \left[-\frac{7}{32} + \frac{\ln 2}{2}\right]\left(1 - \frac{1}{x}\right) - \left[\frac{145}{128} - \frac{7\ln 2}{8}\right]x\right\}, \tag{20}$$

where $x = (\mu_N/\mu_B)(m_p/m_e)(1/ZI)$.

The correction to the hyperfine splitting energy due to a finite size of the nucleus, namely, due the charge and magnetic moment distributions in the nucleus, was introduced by Zemach [40]. The correction is calculated taking into account the electric (G_E) and magnetic (G_M) nuclear form factors and is $-38.72(56)10^{-6}E_F$ for the hydrogen atom in the ground state. The error of $\sim 10^{-6}E_F$ (1 kHz) appears due to the uncertain value of the proton charge radius and prevents a direct QED measurement at a higher accuracy level. However, as mentioned above, the main contributions of the Zemach correction decrease in the 'construction' of the parameter D_{21}.

2.2 Parameter D_{21}

By combining the Breit (10), Zwanziger (15), and Sternheim (20) corrections, we can write the contributions to D_{21} from the terms up to the third order inclusive [$\alpha^3 E_F$, $\alpha^2 \times (m_e/M)E_F$]:

$$D_{21}^{(2)} = \frac{5}{8}(Z\alpha)^2 E_F,$$
$$D_{21}^{(3)} = (Z\alpha)^2 E_F\left\{\frac{\alpha}{\pi}\left(\frac{8}{15}\ln 2 - \frac{7}{10}\right) + \frac{\alpha}{\pi}\left[\left(\frac{16}{3}\ln 2 - 7\right)\ln(Za) - 5.22123\ldots\right] + \frac{m_e}{M}\left[-\frac{9}{8} + \left(\frac{\ln 2}{2} - \frac{7}{32}\right)\left(1 - \frac{\mu_B}{\mu_N}\frac{ZIm_e}{M}\right) - \left(\frac{145}{128} - \frac{7}{8}\ln 2\right)\frac{\mu_N}{\mu_B}\frac{M}{m_e}\frac{1}{ZI}\right]\right\}. \tag{21}$$

In the absence of the fourth-order corrections, the accuracy of this result is worse than the experimental accuracy of measuring D_{21}.

During the last years the higher-order corrections to the hyperfine splitting energy and D_{21} such as $\alpha^2(Z\alpha)^2E_F$ (Fig. 3a), the radiative recoil corrections of the orders $\alpha(Z\alpha)(m_e/M)E_F$ and $(Z^2\alpha)(Z\alpha)(m_e/M)E_F$ (Fig. 3b), and nonradiative recoil corrections $(Z\alpha)^3(m_e/M)E_F$ (Fig. 3c) have been found, and the self-energy [20] and vacuum polarisation [19] corrections have been substantially refined.

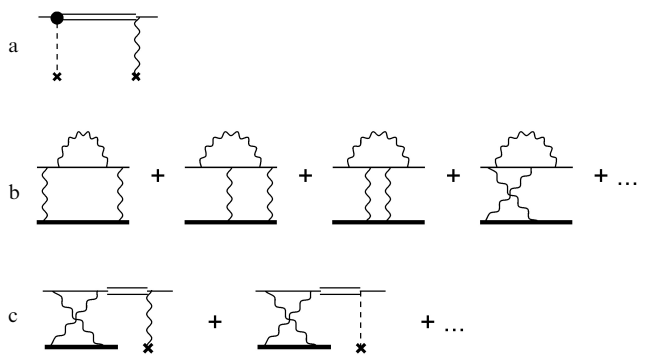

Figure 3. Processes contributing to the corrections to the energy and $D_{21}^{(4)}$. The circle is a vertex operator, the rest of the notation is as in Figs 1 and 2.

These energy contributions were calculated, collected, and analysed in papers of Karshenboim and Ivanov (see, for example, [19]) and can be written as

$$D_{21}^{(4)} = (Z\alpha)^2E_F\left[\frac{\alpha^2}{2\pi^2}\left(\frac{16}{3}\ln 2 - 7\right)\ln(Z\alpha)\right.$$

$$-\frac{\alpha}{\pi}\frac{2m_e}{M}\left(\frac{16}{3}\ln 2 - 7\right)\ln(Z\alpha) + \frac{Z\alpha}{\pi}\frac{2m_e}{M}\left(\frac{4}{3}\ln 2 - 2\right)$$

$$\left.\times\ln(Z\alpha) + \alpha(Z\alpha)(C_{SE} + C_{VP}) + \frac{177}{128}(Z\alpha)^2\right], \qquad (22)$$

where

$$C_{SE}^{(Z=1)} = 2.07(25);\ C_{SE}^{(Z=2)} = 2.01(19);$$

$$C_{VP} = \frac{139}{384} + \frac{13}{24}\ln 2.$$

The residual contribution δD_{21}^{nucl} of hadronic effects is of the same order of magnitude as the fourth-order corrections; this contribution was also estimated in [19]. A small correction δD_{21}^{nucl} can be estimated from the known contributions of hadronic effects to the hyperfine splitting ΔE_{HFS}^{nucl}, which is the difference of the experimental value E_{HFS}^{expt} and the QED calculation neglecting hadronic contributions $E_{HFS}^{QED}(1S)$:

$$\Delta E_{HFS}^{nucl}(1S) = E_{HFS}^{expt}(1S) - E_{HFS}^{QED}(1S). \qquad (23)$$

The calculations give

$$\delta D_{21}^{nucl} = \left(\ln 2 + \frac{3}{16}\right)(Z\alpha)^2\Delta E_{HFS}^{nucl}(1S) +$$

$$+\left(\frac{21}{8} - 2\ln 2 - \frac{3}{8}\zeta\right)\frac{\delta E_N(1S)}{(Z\alpha)^2 m_e}E_F, \qquad (24)$$

where $\delta E_N(1S) = \frac{2}{3}(Z\alpha)^4 m_r^3\langle r_N^2\rangle$ is the correction to the Lamb shift taking a finite size of the nucleus into account [cf. (1)], and $1+\zeta = \langle(r_N^M)^2\rangle/\langle(r_N^E)^2\rangle$ is the ratio of the rms magnetic and charge nuclear radii.

The numerical contributions of different corrections to D_{21} are presented in Table 1. The value of $D_{12}^{theor} = D_{21}^{(2)} + D_{21}^{(3)} + D_{21}^{(4)} + \delta D_{21}^{nucl}$ depends on the ratio of the rms magnetic and charge radii. In principle, this ratio can be estimated from the parameter D_{21}; however, for a modern level of the measurement accuracy of D_{21}, we can assume that $\zeta = 0$.

Table 1. Contributions of different orders to the parameter D_{21} calculated for hydrogen, deuterium, and the $^3He^+$ ion.

Order of contribution to D_{21}	Contribution value/kHz		
	H	D	$^3He^+$
$D_{21}^{(2)}$	47.2220	10.8822	−1152.4390
$D_{21}^{(3)}$	1.7151	0.4233	−36.8234
$D_{21}^{(4)}$	0.0178(25)	0.0043(5)	−1.137(53)
δD_{21}^{nucl}	$-0.002 - 10^{-4}\zeta$	$0.0026(2) - 10^{-4}\zeta$	$0.332(36) + 9\times10^{-3}\zeta$

Note: D_{21}^{theor} is the sum of contributions equal to $48.953(3) - 10^{-4}\zeta$, $11.3125(5) - 10^{-4}\zeta$, and $-1190.067(64) + 9\times10^{-3}\zeta$ for H, D, and $^3He^+$, respectively.

Note that the nonradiative recoil corrections $(Z\alpha)^3\times(m_e/M)E_F$, radiative recoil corrections $\alpha(Z\alpha)^2(m_e/M)E_F$, and two-loop corrections $\alpha^2(Z\alpha)^2E_F$ make substantial contributions to the calculations of the energy levels of hydrogen-like systems. The parameter D_{21} proves to be sensitive to all these corrections, and the elucidation of its structure directly depends on the progress in calculations of the Lamb shift in hydrogen, the hyperfine structure in muonium, and the energy levels of positronium.

3. Measurement of $E_{HFS}(2S)$ in light hydrogen-like systems

The technique for measuring $E_{HFS}(2S)$ in neutral hydrogen-like systems considerably differs from that in $^3He^+$. The possibility of ion localisation in a trap improves the experimental accuracy compared to that in experiments with atomic beams. Although the group of Kleppner has demonstrated the cooling of hydrogen atoms in a magnetic-dipole trap [41], these experiments cannot provide precision spectroscopic measurements due to a high magnetic field strength in the trap. The precision measurements of the hyperfine splitting of metastable levels in hydrogen and deuterium were performed in atomic beams. The first series of experiments was carried out by the group of Kusch at the Columbia University (USA) in 1956 by the method of radio-frequency spectroscopy in a thermal beam [23, 26]. A similar experiment was later performed with the hydrogen atom at the York University (USA) in 2000 [24]. The most accurate values of $E_{HFS}(2S)$ for H and D were obtained in 2000–2004 by the Hänsch group at the Max Planck Institute for Quantum Optics (Germany) by the optical method of two-photon spectroscopy of a cold atomic beam [25, 27].

3.1 Zeeman effect in hydrogen and deuterium

The hyperfine sublevels are split in an external magnetic field due to the interaction of the total atomic momentum $\boldsymbol{F}$ with the external magnetic field B (Zeeman effect). The number of the Zeeman components with different magnetic quantum numbers m_F is $2F+1$, and the dependence of the splitting of the level with the quantum number m_F on the magnetic field is described by the Breit – Rabi formula [31]:

$$\Delta E_{\pm} = -g_{\mathrm{nucl}}\mu_{\mathrm{N}}B \pm \frac{E_{\mathrm{HFS}}}{2}\left(1+\frac{4m_F}{2I+1}\,x+x^2\right)^{1/2}, \qquad (25)$$

$$x = \frac{g_{\mathrm{e}}\mu_{\mathrm{B}} - g_{\mathrm{nucl}}\mu_{\mathrm{N}}}{E_{\mathrm{HFS}}},$$

where E_{HFS} is the hyperfine splitting of the corresponding state.

Figure 4 shows the qualitative picture of the splitting of magnetic sublevels of the 1S and 2S states in hydrogen and deuterium. Because the Fermi energy for deuterium is smaller by a factor of four that for hydrogen, the energy of magnetic sublevels in deuterium is more sensitive to a change in B, which enhances in the general case the sensitivity of measurements in deuterium to the magnetic-field fluctuations.

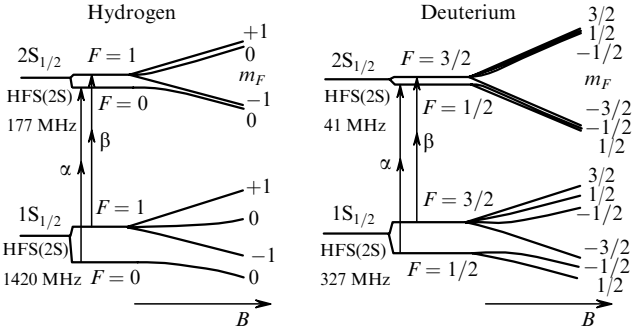

Figure 4. Splitting of the 1S and 2S levels in a magnetic field for hydrogen and deuterium atoms (not in a scale); α and β are two-photon optical transitions between the corresponding hyperfine sublevels of the 1S and 2S states.

3.2 Method of radio-frequency spectroscopy of the 2S level in neutral systems

The radio-frequency method used for the spectroscopy of the 2S state in hydrogen and deuterium atoms was based on the Ramsey spectroscopy in spatially separated fields [23, 26] (measurements in hydrogen and deuterium) and the Rabi method in a travelling wave [24] (measurements in hydrogen). The general scheme of the setup for spectroscopic studies of the 2S level in hydrogen is shown in Fig. 5.

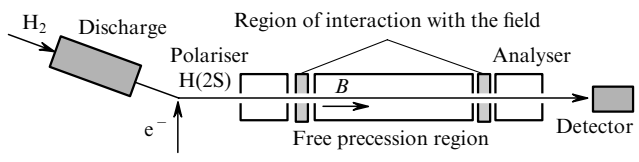

Figure 5. Scheme of the measurement of $E_{\mathrm{HFS}}(2\mathrm{S})$ in hydrogen and deuterium (experimental setup [23]) by the method of Ramsey spectroscopy in spatially separated fields.

The atomic hydrogen produced upon the dissociation of a molecular gas in a radio-frequency discharge was excited by the electron impact to the 2S state. The initial selection over the magnetic sublevels was performed in a strong 575-G magnetic field (polariser), where certain sublevels of the 2S state, whose energy decreases with increasing the magnetic field in the hydrogen atom [for example, such sublevels are 2S ($F=1$, $m_F=-1$) and 2S ($F=0$, $m_F=0$)], are mixed with the adjacent $2\mathrm{P}_{1/2}$ level. Due to a rapid decay of the $2\mathrm{P}_{1/2}$ level to the ground state, the corresponding sublevels of the 2S state are depleted and only the sublevels with $F=1$, $m_F=0$ and $F=1$, $m_F=1$ remain populated.

The prepared beam (the average velocity of the atoms in the beam was 3000 m s^{-1}) was directed to the interaction region with a stable radio-frequency field producing transitions between different hyperfine components. To provide the conditions for exciting the transition between the individual Zeeman sublevels, a homogeneous magnetic field was applied to the interaction region, whose strength could be varied between 10 and 100 mG. After the interaction with the radio-frequency field, which partially populated the $F=0$, $m_F=0$ sublevel, the beam entered a region of free precession where only a homogeneous constant magnetic field was present, and then the beam again propagated through a selective system (analyser). A detector measured the population of the 2S level depending on the detuning of the excited field from the resonance, providing the accurate measurement of the resonance centre. In experiments [23, 24, 30], slightly different technical approaches were used, the setups being similar as a whole.

Therefore, by scanning the excitation-field frequency and monitoring the population of the 2S level, the lines of the allowed transitions between the magnetic sublevels of the hyperfine components of the metastable level were recorded. In the case of the hydrogen atom, these were the lines $2\mathrm{S}(0,0) \leftrightarrow 2\mathrm{S}(1,0)$ and $2\mathrm{S}(0,0) \leftrightarrow 2\mathrm{S}(1,1)$, while in the case of the deuterium atom – the lines $2\mathrm{S}(1/2, -1/2) \leftrightarrow 2\mathrm{S}(3/2, 1/2)$, $2\mathrm{S}(1/2, 1/2) \leftrightarrow 2\mathrm{S}(3/2, -1/2)$, and $2\mathrm{S}(1/2, -1/2) \leftrightarrow 2\mathrm{S}(3/2, -1/2)$. Here, the first number in parentheses corresponds to F and the second one to m_F.

The characteristic line width (of the central interference fringe) was 5 kHz. The main systematic effects affecting the position of the resonance in these radio-frequency experiments were the shift of levels in a magnetic field, the Doppler effect (for experiment [24]), the dynamic Stark shift induced by the radio-frequency field, and the collision shift.

It was found in experiments [23, 26] that the hyperfine splitting frequency of the 2S level in hydrogen was $E^{(\mathrm{H})}_{\mathrm{HFS}}/h = 177556860(50)$ Hz [23] and $E^{(\mathrm{D})}_{\mathrm{HFS}}/h = 40924439(20)$ Hz in deuterium [26]. The values of D_{21} calculated by using these data coincided with the theoretical prediction within one standard deviation. The absolute accuracy demonstrated in experiments with deuterium proved to be better than for hydrogen although the energy of Zeeman components for deuterium is more sensitive to the magnetic field. This is explained by a weak (quadratic) dependence of the average frequency of the $2\mathrm{S}(1/2, -1/2) \leftrightarrow 2\mathrm{S}(3/2, 1/2)$ and $2\mathrm{S}(1/2, 1/2) \leftrightarrow 2\mathrm{S}(3/2, -1/2)$ transitions on the magnetic-field strength and the possibility of the field calibration by the $2\mathrm{S}(1/2, -1/2) \leftrightarrow 2\mathrm{S}(3/2, -1/2)$ transition frequency, which linearly depends on B.

In the radio-frequency experiment [24], the measurement accuracy for the hydrogen atom was improved and the hyperfine splitting frequency $E^{(H)}_{HFS}/h = 177556785(29)$ Hz was obtained. However, the value of D_{21}, calculated by using this result, differed by 1.6σ (σ is the standard deviation) from its theoretical prediction (see Table 1). This discrepancy required the explanation: it could be caused both by the experimental error and the existence of neglected theoretical contributions. In addition, it should be noted that during a few decades separating experiments [23] and [24] the measurement accuracy has been improved only by a factor of two. Experiments [23, 24] with the hydrogen atom were performed by quite similar methods, which stimulated the search for new independent measurement methods.

3.3 Optical method of measuring E_{HFS}(2S) in hydrogen and deuterium

An intense development of the methods of optical spectroscopy and a rapid improvement of the accuracy of optical measurements during the last decade opened up the possibilities for using these methods in the fields where the methods of radio-frequency spectroscopy have been conventionally used. The examples are the measurement of the Lamb shift in hydrogen [42] and studies devoted to the development of frequency standards.

The first measurements of the 1S – 2S transition frequency in the hydrogen atom by the method of two-photon spectroscopy were performed by Hänsch in 1977 [43]. After numerous experiments carried out for many years, the relative accuracy of measuring this frequency achieved 10^{-14}. Such a high resolving power of a hydrogen spectrometer allowed the measurement of the hyperfine splitting of the 2S level with an unprecedented accuracy. In 2003 – 2004, a series of precision measurements of the value of E_{HFS}(2S) in hydrogen and deuterium atoms were performed by the method of two-photon spectroscopy.

Figure 6 shows the scheme of a hydrogen spectrometer which was used for measuring the hyperfine splitting of the metastable level in hydrogen and deuterium. A radiation source was a dye (Coumarin 102) laser emitting ~ 500 mW at a wavelength of 486 nm. The laser frequency was actively stabilised with respect to an external ultrastable thermally and acoustically isolated resonator made of an ULE (Ultra Low Expansion) glass, which has a very small thermal expansion coefficient at room temperature. The finess of the resonator was $\sim 85\,000$ and its free spectral range was 1 GHz. The error signal was obtained by the modulation method of Pound – Drever – Hall [44]. Because the laser radiation was coupled to the resonator through an optical fibre, which introduced considerable noise to the intensity and frequency spectrum of the radiation, the schemes for active compensation for the fibre noise were used. The laser frequency was tuned with respect to the resonator mode frequency with the help of a broadband acousto-optic AOM1 modulator operating in the two-pass scheme in the first diffraction order (Fig. 6). The linewidth of the stabilised laser was ~ 60 Hz, whereas the continuous frequency drift caused by the thermal drift of the resonator length did not exceed 0.5 Hz s^{-1} [44].

The laser radiation was frequency-doubled and directed to the spectroscopic part of the setup located in a vacuum chamber. To provide excitation of a sub-Doppler resonance in the hydrogen (deuterium) atom and increase the excitation-field intensity, the 243-nm radiation was directed to a linear resonator located in the vacuum chamber. The absorption of two counterpropagating photons results in the appearance of a narrow sub-Doppler peak (of the natural width 1.3 Hz). A beam of an atomic gas, preliminary cooled in a cold copper nozzle down to 5 K (the

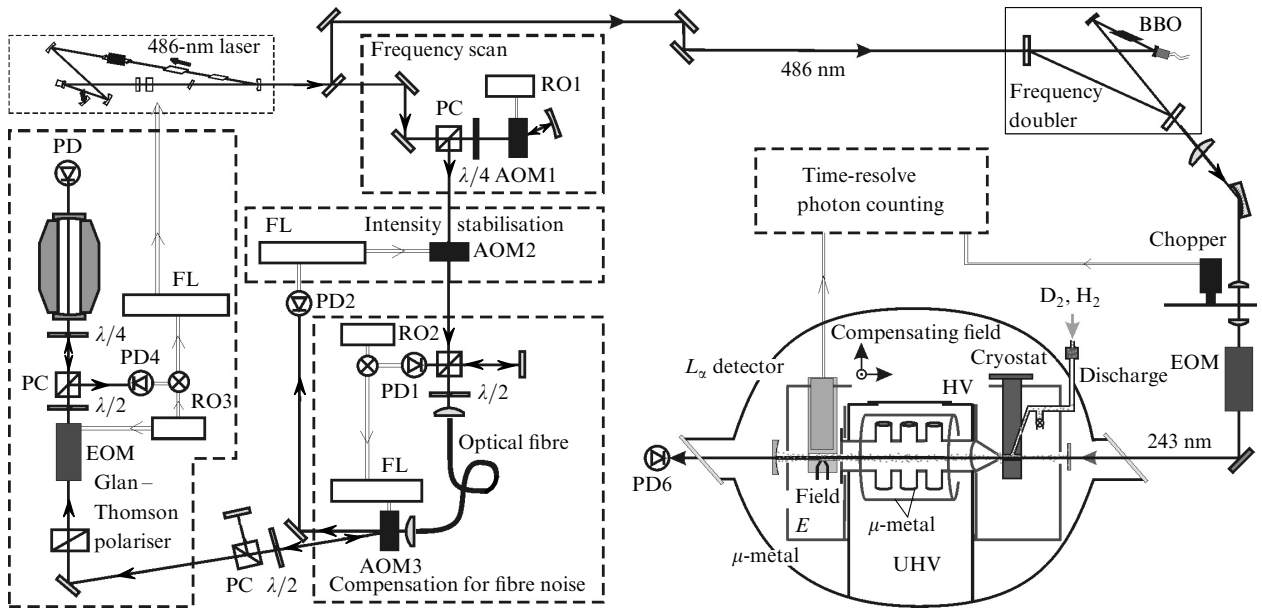

Figure 6. Scheme of the experimental setup for measuring E_{HFS}(2S) in hydrogen and deuterium by the method of two-photon spectroscopy: (PC) polarisation cubes; (AOM and EOM) acousto- and electro-optic modulators; (RO) radio-frequency oscillator; (PD) photodiode; (FL) electronic feedback loop; (HV and UHV) high-vacuum ($\sim 10^{-5}$ mbar) and ultrahigh-vacuum ($\sim 10^{-8}$ mbar) regions; (μ-metal) material with a high magnetic permeability.

average velocity of atoms was 300 m s^{-1}), propagated along the resonator axis to the ultrahigh-vacuum region, where the atoms were excited to the 2S level. The region was protected from external magnetic and electric fields with the help of special shields. The atomic beam intensity could be varied with a valve.

The atoms leaving the excitation region entered the region of a weak electric field E, where the 2S and 1S states mixed efficiently and metastable atoms decayed to the ground state by emitting the L_α photons detected with a photomultiplier. Therefore, by tuning the laser and detecting the number of counts, we could record the 1S–2S two-photon absorption line. In addition, our setup allowed us to perform the spectroscopic study of different velocity groups of atoms from the initial Maxwell distribution by periodically blocking the 243-nm radiation with a chopper and detecting the counts only during the 'dark' phase. The selection over velocities was performed by introducing the time delay τ between the instant of the chopper closing and the count onset (in this case, fast atoms had time to leave the detection region), which allowed the study of atoms with velocities down to 100 m s^{-1}. As the velocity of detected atoms was decreased, the time-of-flight broadening also decreased, as well as the quadratic Doppler effect resulting in the shift and change in the line shape.

In the absence of a magnetic field, the two-photon transition spectrum consists of two components (α and β in Fig. 4), both in the case of the hydrogen and deuterium atoms, because only two-photon transitions with $\Delta F = 0$ and $\Delta m_F = 0$ are allowed. Because in optical experiments there is no need to separate different Zeeman components, the interaction region was shielded from external magnetic fields. The strength of residual fields was ~ 1 mG, which corresponds to the sub-hertz Zeeman splitting. Compared to radio-frequency measurements, this leads to a significant advantage in controlling systematic effects caused by a magnetic field because there is no need to perform extrapolation to the zero field, and the influence of its spatial fluctuations is minimised.

Taking into account the energy level diagrams of atoms presented in Fig. 4, we can write in the absence of a magnetic field:

$$\frac{E_{\mathrm{HFS}}(2\mathrm{S})}{h} = \frac{E_{\mathrm{HFS}}(1\mathrm{S})}{h} + f(\beta) - f(\alpha). \tag{26}$$

Because the value of $E_{\mathrm{HFS}}(1\mathrm{S})$ is known with a high accuracy, to determine $E_{\mathrm{HFS}}(2\mathrm{S})$, it is necessary to find the difference $f(\beta) - f(\alpha)$ of two-photon transition frequencies. The accuracy of the frequency difference measurement is substantially higher than the accuracy of measuring absolute optical frequencies due to the absence of systematic errors in the former case [21].

The optical transition lines were recorded by scanning the laser frequency by changing in steps the frequency f_{AOM} of the generator controlling the AOM1, which was in turn stabilised by the reference signal from an HP5701A cesium standard (Hewlett Packard) having the absolute accuracy no worse than 10^{-12}. The excitation conditions for the α and β components for the both transitions were maintained identical. Figure 7 shows the typical transition lines recorded for a deuterium beam. The typical linewidth for the 121-nm 1S–2S transition is 2 kHz.

The difference of the transition frequencies was determined by using the fact that the optical resonator has a continuous frequency drift. After a linear correction for the frequency drift, the standard Alan deviation σ_{100} for the averaging time 100 s was 10^{-14}. The frequency difference $f(\beta) - f(\alpha)$ was determined by approximating each line by a Lorentzian on the frequency scale (Fig. 7a) and on the time scale. Thus, one point corresponded to each line in the frequency–time scale (Fig. 7b). The difference $f(\beta) - f(\alpha)$ was calculated by making correction for the resonator frequency drift occurring between the instants of recording the transition line centres. While the time between the recordings of the α and β lines in experiments with the hydrogen atom was about 10 min, in the case of deuterium this time was a few seconds. This corresponded to almost simultaneous recording of the lines (Fig. 7), which substantially reduced the error related to the drift correction. As a result, the absolute accuracy of measuring the hyperfine splitting $E_{\mathrm{HFS}}(2\mathrm{S})$ by the optical method in deuterium was noticeably better than that in hydrogen.

Such a differential method significantly reduces the influence of many systematic effects inherent in two-photon

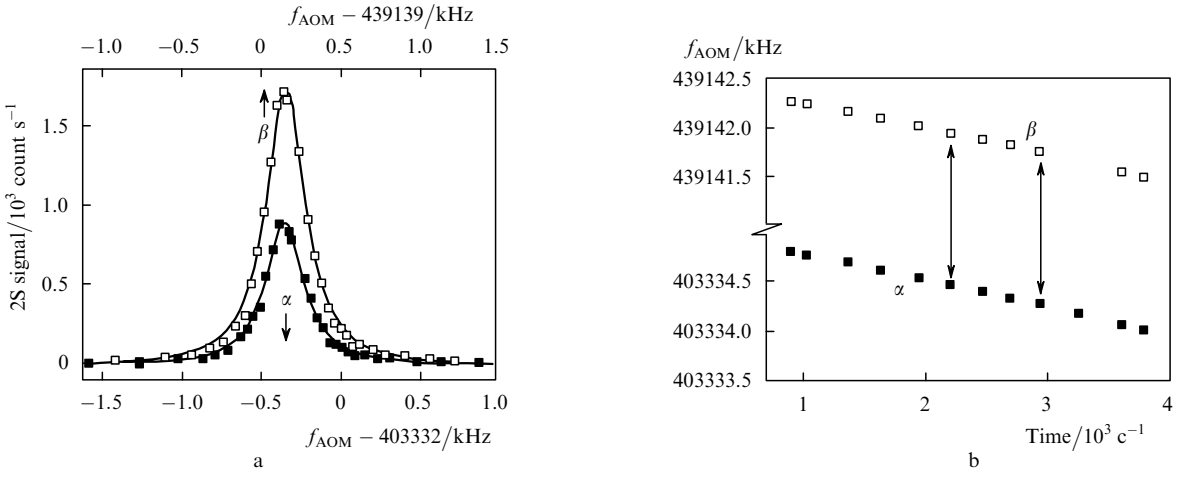

Figure 7. Differential measurement in the deuterium atom. (a) The α and β transition lines recorded for a group of atoms with velocities less than 200 m s^{-1} (the difference in the number of counts is explained by the fact that the statistical weights of the $F = 1/2$ and $F = 3/2$ levels differ twofold) and (b) the result of processing of a series of spectra; a slow frequency drift corresponds to the reference resonator frequency drift.

spectroscopy of atomic beams, which are described in [21]. Thus, the dynamic Stark shift in case of measurement of the hyperfine splitting amounts only to 10^{-6} of its value for optical transitions, while the quadratic Doppler shift and effects related to the asymmetry of the transition lines are compensated. The collision shift of the hyperfine splitting of the 2S level was studied in detail in papers [25, 27]. The experiments were performed at different pressures of a residual gas in the chamber and for different parameters of the atomic beam. Most of the systematic effects in these experiments were at a level of a few hertz.

The hyperfine splitting $E^{(H)}_{HFS}/h$ of the 2S level measured by the optical method in the hydrogen atom was 177 556 860(16) Hz. The accuracy of this measurement is better than that of both known radio-frequency measurements. Note that the 'pure' time of optical measurement is several times shorter than the time required for data accumulation in radio-frequency methods.

The absolute measurement accuracy for the deuterium atom was higher by a factor of three than that achieved in [26]; the value $E^{(D)}_{HFS}/h = 40\,924\,454(7)$ Hz was obtained. No experiments were performed on the spectroscopy of the 2S level in the tritium atom due to a high radioactivity of this atomic system, which prevents the study of atomic tritium beams under usual laboratory conditions.

Therefore, the accuracy of optical methods for neutral systems exceeded that of classic radio-frequency methods. The experimental error can be further reduced by decreasing the velocity of atoms in the beam or by optical cooling the hydrogen atom.

3.4 Measurement of $E_{HFS}(2S)$ in the $^3He^+$ ion

The spin of the even–odd nucleus of the $^3He^+$ ion is 1/2, resulting in the appearance of the two hyperfine components of the S levels of the ion with $F = 0$ and $F = 1$. However, unlike the hydrogen atom, the g-factor of this nucleus is negative and the energy of the $F = 1$ level is lower than that of the $F = 0$ level ($E_F < 0$). Thus, the Zeeman structure of the nS levels of the $^3He^+$ ion proves to be mirror symmetric to the structure of the hydrogen atom shown in Fig. 4.

Experiments on the precision spectroscopy of the 2S level were initiated in the late 1950s at the Columbia University (USA) [29]. The measurement method had much in common with the technique used in radio-frequency experiments with the hydrogen atom [23]. An ion beam was excited to the 2S state by the electron impact and directed to the region of Ramsey spectroscopy in spatially separated fields in the presence of a weak homogeneous magnetic field (cf. Fig. 5). The preliminary selection of atoms on the hyperfine 2S ($F = 0$) sublevel was performed in a polariser to which a weak alternating field at the frequency 13 GHz was applied. The $2S_{1/2}$ level mixed in the field with the short-lived $2P_{1/2}$ level, the 2S ($F = 1$) hyperfine level located closer to the P level being preferably depleted. After the interaction with a stable filed at the frequency 1.083 GHz, which caused the $2S\,(F = 0) \leftrightarrow 2S\,(F = 1)$ transitions, the beam entered a radio-frequency analyser, which was similar in design to the polariser, in which, however, the L_α photons with the wavelength 30 nm (the $2P \rightarrow 1S$ transition) could be detected. The photocurrent value was proportional to the probability of transition between the hyperfine sublevels, which allowed the recording of the Ramsey fringes with the typical width about 100 kHz.

With allowance made for a number of systematic effects (the error was mainly determined by the calibration error of a radio-frequency standard and the dynamic Stark and collision frequency shifts), the splitting $E^{(^3He^+)}_{HFS}(2S)h^{-1} = 1083354990(200)$ Hz was obtained, corresponding to the relative accuracy 2×10^{-7}.

The measurement accuracy was significantly improved in experiments with the $^3He^+$ ions in a trap performed at the University of California (USA) in the mid-1970s [30]. Although the thermal velocity (1500 m s^{-1}) of ions in the trap remained comparable with their thermal velocity in the beam, their localisation resulted in a substantial increase in the free precession time in the Ramsey method. While in the beam experiment this time was determined by the time of flight between the two regions of interaction with the field and restricted the width of interference fringes at a level of 100 kHz, the width of the resonance in the experiments with traps was reduced down to 1 kHz.

In [30], the experimental methods mainly based on beam experiments [29] were used. The ions captured by the trap were selected in the $2S(F = 0)$ state by a radio-frequency pulse at a frequency of ~ 13 GHz. Then, the ions were irradiated by two short successive in-phase microwave pulses at a frequency close to the frequency (1.083 GHz) of the hyperfine transition under study, the width of the resonance being determined by the time interval between pulses. The transition probability was found from the population of the $2S(F = 1)$ level by mixing this level with the $2P_{1/2}$ level in the field with frequency 13 GHz. Therefore, the spectroscopic method virtually coincided with the method described in [29], the only difference being that the propagation of ions through the regions of their interaction with the field was replaced by a sequence of pulses irradiating the localised ions. Note that the laboratory magnetic field in the interaction region was compensated by external coils with a high accuracy, and the ions were confined only due to electrostatic interactions.

The narrow resonance lines and a high signal-to-noise ratio in the experiment made it possible to improve the accuracy of measuring the resonance frequency to a few hertz. The total error was mainly determined by the statistical error (7 Hz), the error due to the inhomogeneity of the magnetic field (3.5 Hz), and the error of measuring the collision shift (3.8 Hz). A periodically calibrated 5105A generator (Hewlett Packard) was used as a frequency standard. The accuracy of the measured value of $E^{(^3He^+)}_{HFS}(2S)/h$ equal to 1083 354 980.7(88) Hz proved to be more than 20 times higher than that in the beam experiment [29], demonstrating the advantage of experiments with ions localised in a trap. Unfortunately, at present the methods for localisation of neutral hydrogen-like atoms in the absence of strong magnetic field are absent.

4. Comparison of experimental and theoretical results

4.1 Hyperfine splitting of the 1S and 2S levels

Table 2 summaries the results of measuring the hyperfine splitting of the 1S and 2S levels in light hydrogen-like systems. The QED calculations of E^{theor}_{HFS} were performed by neglecting the nuclear structure (according to [19]).

One can see that the discrepancy between the experimental and calculated values for hadronic systems is

Table 2. Hyperfine splitting in light hydrogen-like systems.

Atom	Atomic state	$E_{\mathrm{HFS}}^{\mathrm{expt}}\,h^{-1}$/kHz	Reference	$E_{\mathrm{HFS}}^{\mathrm{theor}}\,h^{-1}$/kHz	$n^3\Delta E\,E_F^{-1}/10^{-6}$
H	1S	1420 405 751 768(1)	[13]	1 420 452	−33
D	1S	327 384 352 522(2)	[22]	327 339	138
He^+	1S	−8665 649 867(10)	[28]	−867 569	222
H	2S	177 556 860(50)	[23]	177 562.7	−32
H	2S	177 556 785(29)	[24]	177 562.7	−33
H	2S*	177 556 860(16)	[25]	177 562.7	−32
D	2S	40 924 439(20)	[26]	40 918.81	137
D	2S*	40 924 454(7)	[27]	40 918.81	138
He^+	2S	−1083 354 981(9)	[30]	−1083 594.7	221
He^+	2S	−1083 354 99(20)	[29]	−1083 594.7	221
Mu	1S	4463 302 78(5)	[15]	4463 302.91(56)	0.0(1)
Ps	1S	203 389 100(700)	[16]	203 391 900(500)	−13(44)

Note: The asterisk refers to optical measurements; $\Delta E = E_{\mathrm{HFS}}^{\mathrm{expt}} - E_{\mathrm{HFS}}^{\mathrm{theor}}$; theoretical estimates are taken from [19].

$10^{-5} - 10^{-4}$ of the splitting value, which is explained by a finite size of the nucleus. This is confirmed by the corresponding values of the ground-state hyperfine splitting in leptonic systems, muonium and positronium. The experimental value of $E_{\mathrm{HFS}}^{\mathrm{theor}}(1S)$ for muonium, which is known with an extremely high accuracy, agrees with the theoretical value with an accuracy of 10^{-7}, thereby making this system a very convenient object for QED tests in hyperfine-splitting calculations [1]. However, as mentioned in Introduction, the sensitivity of these tests is limited by the measurement error of the m_μ/m_e ratio, which determines to a great extent the accuracy of measuring $E_{\mathrm{HFS}}^{\mathrm{theor}}(1S)$ in muonium.

4.2 Parameter D_{21}

The study of the parameter D_{21} allows the testing of certain QED corrections to the hyperfine-splitting energy, which depend on the principal quantum number n. By combining the values of $E_{\mathrm{HFS}}(1S)$ and $E_{\mathrm{HFS}}(2S)$ in H, D, and $^3He^+$, we can obtain the values of D_{21} for these systems (Table 3). The experimental data are compared with theoretical values in Fig. 8. Most of the experimental results correspond to the theoretical predictions within a standard deviation. Because the results have been obtained by independent methods, it is reasonable to average the experimental values taking into account the weight coefficients specified by the squares of corresponding standard deviations. We have found that the parameter D_{21} for hydrogen, deuterium, and the helium ion is 49.00(17), 11.267(52), and −1189.979(71) kHz, respectively. In this case, $\sigma/E_F = 0.12 \times 10^{-6}$, 0.16×10^{-6}, and 0.01×10^{-6}, respectively.

The error was calculated in a standard way. Note that the result of the beam experiment [29] for the helium ion virtually does not affect the average value and its error. However, in the case of the hydrogen atom, the scatter of the data exceeds the standard deviations of individual measurements (Fig. 8), and the resulting error is determined by the scatter of the experimental data.

The average values of D_{21} for light hydrogen-like atoms are in good agreement with theoretical predictions and make it possible to perform QED tests for calculating the hyperfine splitting in such systems at a level of $10^{-7} - 10^{-8}$. One can see that most of the beam experiments allow the testing of the correction to D_{21} at a level of 10^{-7}, whereas the result [30] obtained for the helium ion confined in a trap further increased the sensitivity of QED tests by an order of magnitude. In turn, the possibilities of optical methods, which allowed the measurement of D_{21} in neutral systems with an unprecedented accuracy, are far from being exhausted and promise a further progress in this field.

Table 3. Comparison of the experimental and theoretical values of D_{21} in light systems.

Atomic system	$D_{21}^{\mathrm{expt}}\,h^{-1}$/kHz	References	$D_{21}^{\mathrm{theor}}\,h^{-1}$/kHz	$\Delta D_{21}\,E_F^{-1}/10^{-6}$	$\sigma\,E_F^{-1}/10^{-6}$
H	49.12(13)	[25]*/[13]	48.953(3)	0.12	0.08
	48.53(24)	[24]/[13]		−0.29	0.16
	49.13(40)	[23]/[13]		0.12	0.28
D	11.280(56)	[27]*/[22]	11.3125(5)	0.10	0.17
	11.160(160)	[26]/[22]		−0.46	0.49
$^3He^+$	−1189.979(71)	[30]/[28]	−1 190.067(64)	0.01	0.01
	−1190.1(16)	[29]/[28]		−0.03	0.18

Note: Results correspond to different measurements of $E_{\mathrm{HFS}}(2S)$ and $E_{\mathrm{HFS}}(1S)$ (references in front and behind the slash, respectively), the theoretical values are taken from [19]; $\Delta D_{21} = D_{21}^{\mathrm{expt}} - D_{21}^{\mathrm{theor}}$, σ is the total experimental and theoretical error equal to a standard deviation; the asterisk refers to optical measurements.

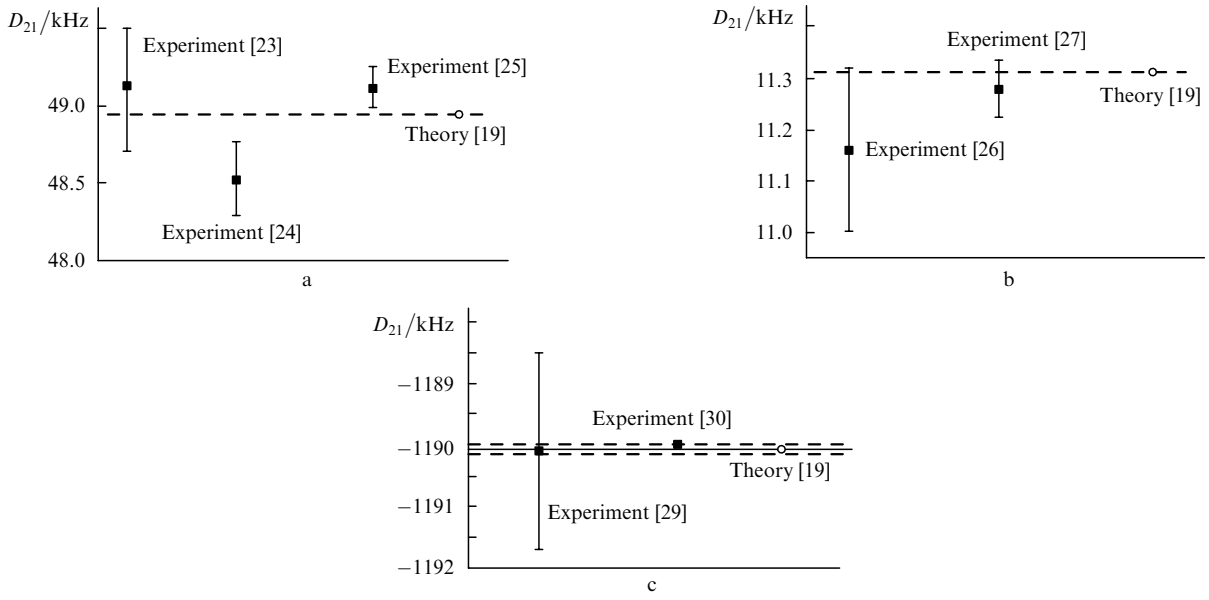

Figure 8. Comparison of experimental and theoretical values of D_{21} for hydrogen (a), deuterium (b), and the $^3He^+$ ion (c). The dashed straight lines correspond to the error of the theoretical value (one standard deviation).

5. Conclusions

The results of measuring the hyperfine splitting of the 2S level in light hydrogen-like systems have been analysed. The theoretical approaches used in the hyperfine-splitting calculation were considered and the method was presented for calculating the specific parameter D_{21}, which is free from a leading contribution of corrections appearing due to a finite size of the nucleus.

Analysis of the results of studying the hyperfine splitting of the metastable level in the hydrogen atom has shown that the possibilities of radio-frequency methods using neutral atomic beams are most likely exhausted and optical methods play a leading role in this field at present.

A substantial advantage in accuracy achieved in the spectroscopy of atomic systems captured in traps (as demonstrated for the $^3He^+$ ion) is inaccessible for hydrogen and deuterium so far. However, the absolute accuracy of optical measurements in hydrogen and deuterium is at the same level as for the radiospectroscopy of the $^3He^+$ ion in a trap.

The values of D_{21} obtained from the measurements of $E_{HFS}(2S)$ in light systems are in good agreement with the QED theoretical values calculated up to the terms of the orders $\alpha^2(Z\alpha)^2 E_F$, $\alpha(Z\alpha)(m_e/M)E_F$, and $(Z\alpha)^3(m_e/M)E_F$ inclusive. Note that unlike the QED tests, which are based on the hyperfine-spitting study, in this case only the corrections depending on the principal quantum number n are tested. The sensitivity of QED tests based on the study of the parameter D_{21} in hadronic systems is comparable with that of the investigation of the ground-state hyperfine splitting in muonium, which is a leptonic system.

Tests based on the study of the parameter D_{21} supplement harmonically the picture of precision QED tests of bound states in the calculation of light atomic systems. The calculations of the Lamb shift, the hyperfine structure, the parameter D_{21}, and the g-factor of a bound electron represent the closed interaction of the bound electron with the field, allowing a comparison with precision experimental data. A deeper insight in the nature of this interaction requires the refinement of the experimental data and the search for new objects that can be accurately theoretically described.

Acknowledgements. The author thanks S.G. Karsheboim, V.G. Ivanov, M. Fischer, P. Fendel, T. Udem, V. Shabaev, U. Jentschura, and T. Hänsch for active discussions of the paper. The author is grateful to all his colleagues from the Max Planck Institute on Quantum Optics (Germany) collaborating in optical experiments on the spectroscopy of hydrogen and deuterium atoms. This work was partially supported by the Alexander von Humboldt Foundation, the President of the Russian Federation Program for Supporting Young Russian Scientists and Leading Scientific Schools (Grant No. 1254.2003.2), the German Research Community (DFG Grant No. 436RUS113/769/0-1), and the Russian Foundation for Basic Research (Grant No. 04-02-17443).

References

1. Eides M.I., Grotch H., Shelyuto V.A. *Phys. Rep.*, **342**, 63 (2001); hep-ph/0002158.
2. Biraben F. et al., in *The Hydrogen Atom. Precision Physics of Simple Atomic Systems* (Ed. by S.G. Karshenboim) (Berlin-Heidelberg: Springer, 2001) pp 18 – 41.
3. Drake G.W.F. *Can. J. Phys.*, **80**, 1195 (2002).
4. Mohr P.J., Taylor B.N. *Rev. Mod. Phys.*, **72**, 351 (2000).
5. Mohr J.P., Taylor B.N. *Phys. Today*, **54** (3), 29 (2001).
6. Beier T. et al. *Phys. Rev. Lett.*, **88**, 011603 (2002); Beier T., Indelicato P., Shabaev V.M., Yerochin V.A. *J. Phys. B: At. Mol. Opt. Phys.*, **36**, 1019 (2003).
7. Farnham D.L., Van Dyck R.S. Jr., Schwinberg P.B. *Phys. Rev. Lett.*, **75**, 3598 (1995).
8. Janssens T. et al. *Phys. Rev.*, **142**, 922 (1966).
9. Simon G.G. et al. *Nucl. Phys. A*, **364**, 285 (1981).
10. Udem Th. et al. *Phys. Rev. Lett.*, **79**, 2646 (1997).
11. Rosenfelder R. *Phys. Lett. B*, **479**, 381 (2000).
12. Kottmann F. et al., in *Proc. Conf. QED'2000* (Ed. by G. Cantatore) (New York: AIP, 2001) Vol. 564, p. 13.

13. Verdú J.L. et al. *Can. J. Phys.*, **80**, 1233 (2002).
14. Liu W. et al. *Phys. Rev. Lett.*, **82**, 711 (1999).
15. Ritter M.W., Egan P.O., Hughes V.W., Woodlev K.A. *Phys Rev. A*, **30**, 1331 (1984).
16. Farley F.J.M., Picasso E., in *Quantum Electrodynamics* (Ed. by T. Kinoshita) (Singapore: World Scientific, 1990) p. 479.
17. Ramsey N., in *Quantum Electrodynamics* (Ed. by T. Kinoshita) (Singapore: World Scientific, 1990) p. 673; *Hyp. Interactions*, **81**, 97 (1993).
18. Shabaev V.M. et al. *Phys. Rev. A*, **65**, 062104 (2002).
19. Karshenboim S.G., Ivanov V.G. *Phys. Lett. B*, **524**, 259 (2002); *Euro. Phys. J. D*, **19**, 13 (2002).
20. Yerochin V.A., Shabaev V.M. *Phys. Rev. A*, **64**, 012506 (2001).
21. Niering M. et al. *Phys. Rev. Lett.*, **84**, 5496 (2000).
22. Wineland D.J., Ramsey N.F. *Phys. Rev. A*, **5**, 821 (1972).
23. Heberle J.W., Reich H.A., Kusch P. *Phys. Rev.*, **101**, 612 (1956).
24. Rothery N.E., Hessels E.A. *Phys. Rev. A*, **61**, 044501 (2000).
25. Kolachevsky N. et al. *Phys. Rev. Lett.*, **92**, 033003 (2004).
26. Reich H.A., Heberle J.W., Kusch P. *Phys. Rev.*, **104**, 1585 (1956).
27. Kolachevsky N., Fendel P., Karshenboim S.G., Hänsch T.W. *Phys. Rev. A*, **70**, 062503 (2004).
28. Schluesser H.A. et al. *Phys. Rev.*, **187**, 5 (1969).
29. Novick R., Commins E. *Phys. Rev.*, **111**, 822 (1958).
30. Prior M.H., Wang E.C. *Phys. Rev. A*, **16**, 6 (1977).
31. Bethe H.A., Salpeter E.E. *Quantum Mechanics of One- and Two-Electron Atoms* (New York: Academic Press, 1957; Moscow: Fizmatgiz, 1960).
32. Breit G. *Phys. Rev.*, **35**, 1447 (1930); **39**, 616 (1932).
33. Berestetskii V.B., Lifshits E.M., Pitaevskii L.P. *Quantum Electrodynamics* (Oxford: Pergamon Press, 1982; Moscow: Nauka, 1989).
34. Kroll N., Pollok F. *Phys. Rev.*, **84**, 594 (1951); **86**, 876 (1952).
35. Karplus R., Klein A. *Phys. Rev.*, **85**, 972 (1952).
36. Blundell S.F., Cheng K.T., Sapirstein J. *Phys. Rev. Lett.*, **78**, 4914 (1997).
37. Eides M., Shelyto V. *Phys. Rev. A*, **52**, 954 (1995); *Pis'ma Zh. Eksp. Teor. Fiz.*, **61**, 465 (1995).
38. Kinoshita T., Nio M. *Phys. Rev. Lett.*, **72**, 3803 (1994).
39. Sternheim M. *Phys. Rev.*, **121**, 211 (1963).
40. Zemach C. *Phys. Rev.*, **104**, 1771 (1956).
41. Cesar C.L., Kleppner D. *Phys. Rev. A*, **59**, 4564 (1999).
42. Weitz M., Schmidt-Kaler F., Hänsch T.W. *Phys. Rev. Lett.*, **68**, 1120 (1992).
43. Hänsch T.W. *Laser Spectroscopy III* (Ed. by J.L. Hall, J.L. Carlsten) (Berlin – New York: Springer, 1977) Vol. 7, p. 423.
44. Fischer M., Kolachevsky N., Karshenboim S.G., Hänsch T.W. *Can. J. Phys.*, **80** (11), 1225 (2002).